

Giant mobility of surface-trapped ionic charges following liquid tribocharging

Zouhir Benrahla¹, Tristan Saide¹, Louis Burnaz¹, Emilie Verneuil¹,
Simon Gravelle², Jean Comtet^{1*}

¹*Soft Matter Sciences and Engineering, ESPCI Paris, PSL University, CNRS, Sorbonne
Université, 75005 Paris, France*

²*Univ. Grenoble Alpes, CNRS, LIPhy, 38000 Grenoble, France*

[*jean.comtet@espci.fr](mailto:jean.comtet@espci.fr)

The sliding motion of aqueous droplets on hydrophobic surfaces leads to charge separation at the trailing edge, with implications from triple-line friction to hydrovoltaic energy generation. Charges deposited on the solid surface have been attributed to stem from ions or electrons ripped off from the liquid drop. However, the dynamics and exact physicochemical nature of these surface-trapped charges remains poorly explored. Here, we take advantage of a scanning-based electrostatic mapping technique, to directly quantify the spatiotemporal dynamics of surface deposited charges in the wake of droplets sliding on hydrophobic surfaces. We confirm the ionic nature of these interfacially trapped charges, and evidence that they undergo very fast bidimensional diffusive transport, gliding with low friction at the solid/gas interface. We rationalize our observations through molecular dynamics simulation of hydrated ions adsorbed on solid surfaces, revealing a peculiar transport mechanism limited by purely interfacial friction of the ionic solvation shell with the solid surface. By uncovering the unexpected dynamics of these *ionic puddles* - a new state of interfacial ionic matter - our findings have general implications for molecular-scale ionic transport and electrified matter at interfaces.

Tribocharging - the process by which surfaces charge following frictional contact - is a long-standing issue in physics and material science [1], with broad implications ranging from the mundane experience of “static electricity” [2] to protoplanetary formation from spatial dust aggregation [3]. Amongst the diverse electrification processes which usually involve contacts between solid-state insulating or conducting materials, *liquid tribocharging* stands aside, with electrification occurring through the sliding motion of a liquid water droplet on a solid hydrophobic surface. In this peculiar situation, surface-deposited charges are thought to originate from bulk ionic carriers present in the liquid drop [4], [5], while the gliding motion at the deformable contact line couples to the charge deposition processes, leading to new dissipation pathways [6]–[8]. Liquid tribocharging has thus raised considerable interests in the recent years [9], [10], being commonly experienced in a variety of situations of applied interests, such as pipetting [11], [12], self-charging of spray [13], droplet jumping [14] and directional droplet transport [15], as well as in the development of nanogenerators with promising performances [16], [17].

At a mechanistic level, charging is thought to stem from ions adsorbed specifically on the solid/liquid interface inside the droplet, which are deposited on the solid surface due to their sluggish dynamics during droplet dewetting [4], [5]. Interestingly, electrons have also been put forward as possible charge-carriers [18]–[20]. However, due to the challenges associated with accessing interface-specific information at appropriate spatial and temporal resolution, the nature, physicochemical state and dynamics of the charges deposited on the surface of the solid has remained largely unexplored. In particular, most studies approaching these questions focused either on the droplet charge or spatially-averaged surface charge (except for an early seminal work [21]), therefore providing a partial and incomplete picture of the deposited charges dynamics.

Here, we harvest an in-situ scanning based potential mapping approach, to reveal the spatial and temporal evolution of surface-deposited charges following the sliding of droplets on hydrophobic surfaces. We first evidence that surface charging at low droplet numbers occurs in a heterogeneous fashion with patches of alternating signs. At large droplet numbers, we observe a monotonously decreasing potential, whose sign and magnitude can be reversibly tuned by the bulk droplet pH, pointing to the role of water self-ion and dissolved CO₂ in the surface charging mechanism. Remarkably, the charges initially deposited along the wake of the droplet tend to spread apart on the solid surface over time, consistent with a bidimensional diffusion process associated with ultra-high 2D gliding mobility exceeding that of standard salt in bulk water. We rationalize these experimental observations through MD simulations of hydrated ions adsorbed on model hydrophobic surfaces, evidencing that interfacial mobility in this peculiar situation becomes uncorrelated to bulk ionic diffusion, but leads to the emergence of an interface-specific dissipative process set by the contact of the ionic hydration layer with the surface of the solid. Our findings have broad implications and open up many exciting avenues, from the role of water and ionic adsorbates in solid-solid electrification, to the fundamentals raised by the dynamics of these *ionic puddles* – a new state of interfacial ionic matter.

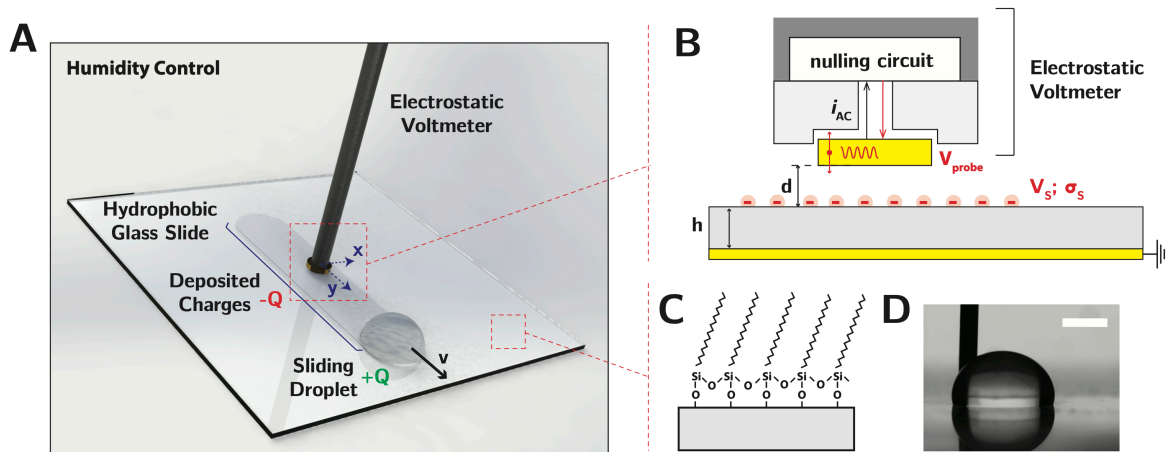


Figure 1. Large-scale surface potential mapping. (A) Schematic of the set-up used for the spatio-temporal characterization of surface charging by sliding droplets. A droplet of liquid impacts and slides with velocity $v \approx 0.5 \text{ m}\cdot\text{s}^{-1}$ over a tilted hydrophobic glass surface. The local density of surface deposited charges σ_S [$\text{C}\cdot\text{m}^{-2}$] induces a surface potential V_S [V] which is spatially mapped by a scanning electrostatic voltmeter. (B) Schematic principle for surface potential mapping using the electrostatic voltmeter. Surface deposited charges with density σ_S are represented in red and induce a surface potential V_S . A metallic probe (potential V_{probe}) oscillates at a distance $d = 700 \mu\text{m}$ from the solid surface, inducing an AC current, proportional to the voltage difference $|V_S - V_{\text{probe}}|$. A nulling circuit adjusts the probe potential so that $V_S = V_{\text{probe}}$. The hydrophobic glass plate holding the deposited charges has a thickness $h = 2 \text{ mm}$ and is grounded on the backside (yellow electrode). (C) Schematic of the surface chemistry, with C₁₈ chains grafted to the glass surface, rendering the surface hydrophobic (see SI.S1 for details on substrate preparation). (D) Image of a water droplet sitting on the surface. Scale bar is 2 mm.

Surface potential mapping reveals heterogeneous charge deposition by sliding droplets

To probe the spatial and temporal dynamics of surface-deposited charges following droplet sliding, we take advantage of a scanning-based electrostatic potential mapping technique, pictured in Fig. 1 and detailed in SI.S2. Briefly, the aqueous droplets impact and slide on a tilted hydrophobic surface, consisting of a glass plate grafted with a self-assembled monolayer of long C₁₈ chains (Fig. 1C-D, and SI.S1). By sliding on such a hydrophobic surface, droplets acquire a net positive charge which is readily detected through the measurement of their discharge current on a downstream electrode (Fig. S2, [4]–[6]), leading presumably to the deposition of charges of opposite signs on the solid surface. These deposited surface charges of density σ_S [$\text{C}\cdot\text{m}^{-2}$] lead to the build-up of a surface potential V_S [V], with $\sigma_S = (\epsilon_r \epsilon_0 V_S)/h$,

where $\epsilon_r \approx 4.8$ [-] the relative dielectric constant of the glass, ϵ_0 [F.m⁻¹] the vacuum permittivity and h [m] the glass plate thickness. This surface potential can be spatially mapped by a non-contact field-compensating electrostatic voltmeter with a metallic electrode (diameter 790 μm) oscillating above the surface. In this geometry, the probe oscillation induces an AC capacitive current i_{AC} proportional to the probe/surface potential difference $|V_{\text{probe}} - V_S|$, which is nullified to access the local surface potential V_S and associated surface charge density σ_S . By scanning the electrostatic voltmeter above the surface, surface potential maps are readily obtained.

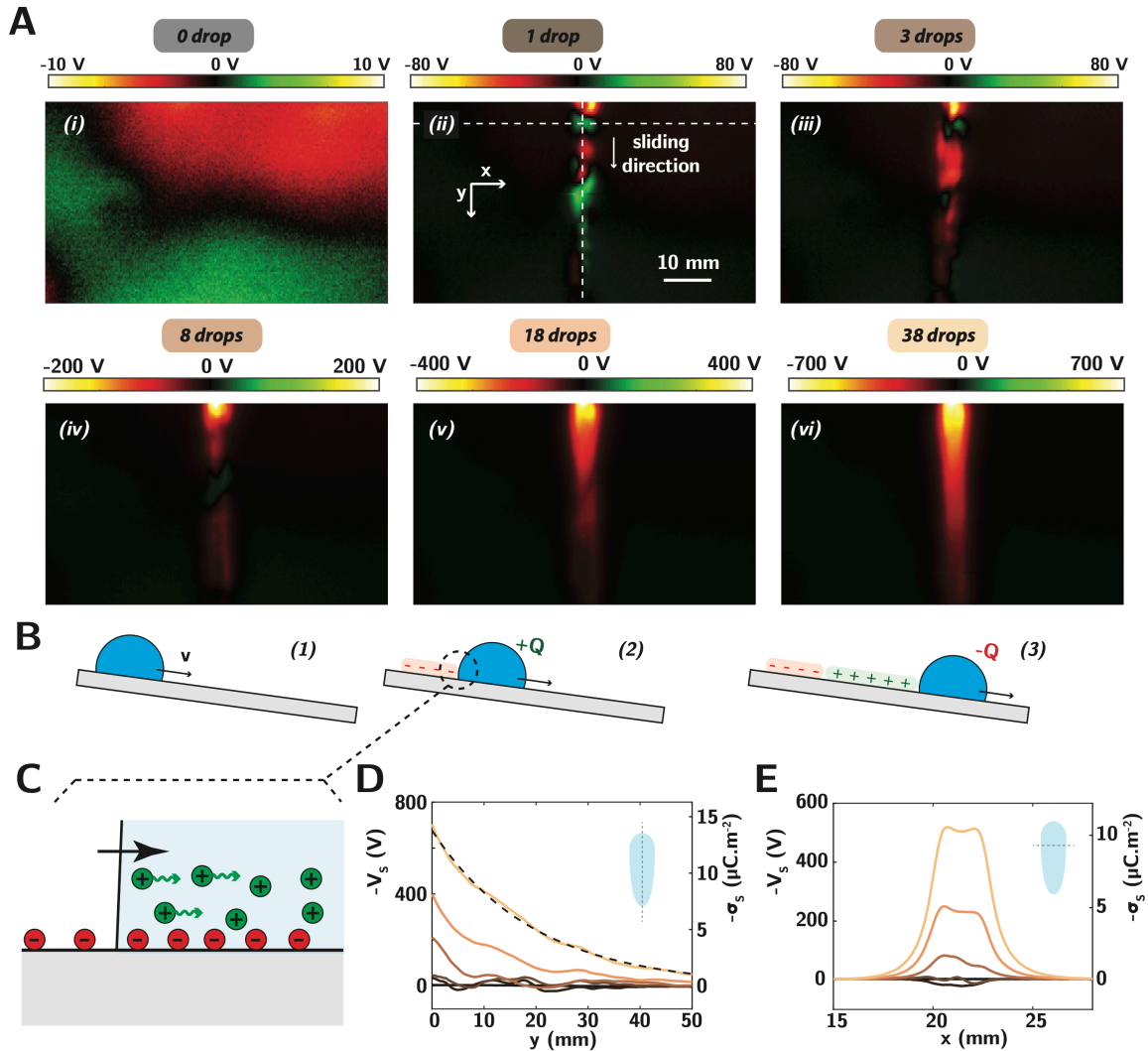


Figure 2. Heterogeneous spatial surface charging following liquid triboelectrification. (A) Evolution of the surface potential for increasing droplet number. The point of impact of the drop is situated at the top of the image. The interval time between each scan is of the order of 20 minutes and the droplets are launched sequentially on the same path at a rate of ≈ 1 droplet per second. Droplets are composed of deionized water of pH ~ 5.5 . (B) Schematic of the observed charge oscillation during droplet sliding. The droplet is initially neutral and gets positively charged (+Q, green) while depositing negative charges (red) to the surface. Upon accumulation of excess positive charges in the drop, positive charges (green) are transferred to the surface, and the drop charge relaxes to negative values, leading to the observed charge oscillations. (C) Zoom-in at the triple-line on the rear of the droplet. Inside of the droplet, negative charges (red) adsorbed to the interface are screened by counter-ions in the liquid (green). Upon dewetting of the triple line, negative charges adsorbed to the solid/liquid interface are transferred to the solid/gas interface. (D, E) Spatial evolution of the surface potential along (D) and perpendicular (E) to the drop sliding path, on a surface charged from 0 to 38 drops (under the same conditions as in (A)). The dashed line in D is an exponential fit. Insets are top views of the droplet patterns.

We first investigate in Fig. 2A how the local surface charge state varies upon increasing the number of sliding droplets. We systematically start our experiments by annealing surfaces at 150°C, allowing us to obtain an initially homogeneous surface state free of residual surface charges, as shown in Fig. 2A, *i*, where the RMS voltage is lower than 2 V. Following sliding of the first droplet (Fig. 2A, *ii*), we clearly evidence the deposition of charges in the wake of the droplet trajectory (vertical dashed line). Unexpectedly, while previous ensemble measurements highlighted a systematically positive charging of the droplet, interpreted as the deposition of purely negative charges onto the surface [4], [6], [22], our local measurements evidence that charges deposition occurs through patches of alternating signs. Starting with the deposition of negative charges at the impact point (top of the image, red region), the deposited charge shows clear oscillations along the vertical y-axis reaching successively positive (green) and negative (red) values. As schematically represented in Fig. 2B, such alternating charge patches might stem from the evolution of the droplet charge during sliding: following impact and initial sliding, the drop becomes positively charged and its potential rises, which ultimately shifts the sign of the deposited charges to positive values, etc. Upon increasing the number of sliding droplets (Fig. 2A, *ii* to *iv*) positively charged domains in green are progressively smeared out. At the same time, the surface becomes increasingly negatively charged until reaching uniformly negative values (Fig. 2A, *v* and *vi*), a clear signature of the preferred transfer of negative charges from the solid/liquid to the solid/gas interface.

A coarse mechanism for the charging process is schematically represented in Fig. 2C. Inside the droplet, the solid/liquid interface bears a negative charge originating from specific ionic adsorption (red negative charges), which are screened by counterions in the liquid (green positive charges) over nanometric distances [23]. Upon displacement of the triple-line, counterions are convected by the liquid, while some surface-adsorbed ions are transferred from the solid/liquid interface to the solid/gas interface, due to their sluggish dynamics induced by their interactions with the surface. It thus appears interesting to compare the charge densities deposited on the solid surface with those generated through ionic adsorption in the solid. The surface potential at the impact point is found to be of the order of 30 V, corresponding to surface charge density of $\approx 0.5 \mu\text{C} \cdot \text{m}^{-2}$, several orders of magnitude smaller than the surface charge density of 0.1-1 $\text{mC} \cdot \text{m}^{-2}$ expected to develop at similar hydrophobic surface in deionized water [24], demonstrating the very low probability associated with this charge ripping process. Conversely, at large drop numbers, the absolute surface potential can reach up to 1800 V at the impact point (the saturation limit of our instrument) associated with absolute charge densities up to $35 \mu\text{C} \cdot \text{m}^{-2}$. In this limit, the potential decays approximately exponentially along the drop path, with a characteristic distance of $\approx 20 \text{ mm}$ (Fig. 2D, black dashed line), a feature reminiscent of previous observations of the charge of the droplets that were found to saturate with the length they were allowed to slide [4], [6]. In the direction transverse to the sliding path (Fig. 2E), the surface potential is approximately constant along the wake of the drop, demonstrating the occurrence of homogeneous charging, although some slight over-charging at the edges of the wake can be observed far from the impact point (Fig. 2F).

Surface trapped charges glide with ultra-low friction on the solid surface.

Observing this peculiar trapping process raises the question of the dynamics of the surface deposited charges. We thus track the long-term spatial and temporal evolution of the surface potential profile following charging of the surface by a large number of droplets (SI Fig. S1). As shown in Fig. 3A, the charges initially deposited and confined along the drop wake are found to spread out on the surface over time, suggesting their large mobility through diffusion over several hours. To further quantify this transport process, we report in Fig. 3B, the temporal evolution of the surface potential profile perpendicular to the drop wake close to the impact point, evidencing again the spreading of the deposited charge. Due to the geometry of the

deposited charge patch, surface diffusion can be well-described by a 1D transport process (SI. S3) and quantified by evaluating the temporal evolution of the Full Width at Half Maximum Δ of each profile. As reported in Fig. 3C, following an initial sublinear evolution associated with the finite width of the deposited charge patch, Δ^2 shows a clear linear scaling with time, consistent with a purely diffusive process characterized here by a surface diffusion coefficient $D_{\text{surface}} \approx 2.6 \cdot 10^{-9} \text{ m}^2 \cdot \text{s}^{-1}$. This linear scaling indicates in particular the negligible repulsive electrostatic interactions between the deposited charges. For surface charge densities $\sigma \approx 35 \mu\text{C} \cdot \text{m}^2$, the typical distance between charge reaches $l \sim (\sigma/e)^{-1/2} \approx 70 \text{ nm}$, which is indeed slightly larger than the Bjerrum length $l_B \sim e^2/(4\pi\epsilon_0 k_B T) \approx 57 \text{ nm}$ evaluated in air (with $\epsilon_r \approx 1$), which defines the typical distance at which thermal motion overcomes electrostatic interactions.

Such diffusion process was evidenced on several samples, with slight variations from surface to surface, leading to typical diffusion coefficients ranging from $1 \cdot 10^{-9}$ up to $7 \cdot 10^{-9} \text{ m}^2 \cdot \text{s}^{-1}$. Surprisingly, such values are found to be *of the same order or even larger* than the typical diffusion coefficient of simple ions in bulk water, taking as a reference a diffusion coefficient $D_{\text{Na}^+} \approx 1.4 \cdot 10^{-9} \text{ m}^2 \cdot \text{s}^{-1}$ for sodium ions at 25°C [25]. The remarkably high mobilities are unexpected for an interfacially limited transport, in which wall-induced friction is typically expected to slow down the dynamics compared to a bulk system. A mechanism consistent with the high mobility of the ions is proposed below.

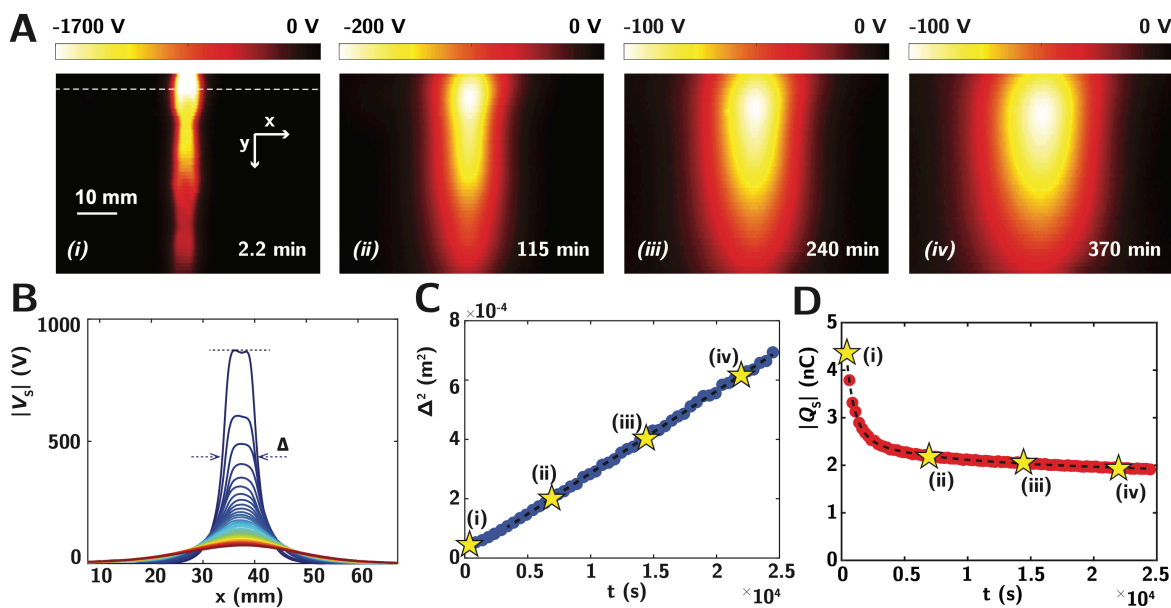


Figure 3. Surface charge diffusion. (A) Temporal evolution of a patch of surface charges, showing its progressive spreading on the surface of the solid over increasing time. The initial patch is formed by sliding 35 droplets (deionized water, pH ~ 5.5) at a rate of ≈ 1 droplet/second. (B) Temporal evolution of the surface potential transverse to the sliding droplet path, characterizing the Full Width at Half Maximum Δ for the initial profile in dark blue. The time-interval between each curve is 502 s and the elapsed time between the initial and final profiles is $2.5 \cdot 10^4 \text{ s} \approx 7$ hours. (C) Evolution of Δ^2 as a function of time. (D) Relaxation of the total surface deposited charge $|Q_s|$ over time. The dashed line is an empirical fit combining exponential and power-law relaxation (see Fig. S5 for details). In (C) and (D), the stars indicate the timestamps corresponding to the four images in (A).

Another remarkable aspect of this charge transport process lies in the exceptionally large stability of the deposited surface charge, as demonstrated in Fig. 3D, where we present the temporal evolution of the total charge deposited on the surface $|Q_s|$, obtained by integrating the total charge density of the imaging area. We observe in this figure a short-term exponential-like relaxation with a characteristic time of 15 to 20 minutes, after which the charge transitions to a much slower relaxation process (see Fig. S5 for details). We propose that this transient

relaxation of the surface potential is due to the equilibration of the physicochemical state of the deposited charge, possibly caused by the progressive build-up of a physisorbed water shell around the ions, which may screen the induced field and surface potential. The long remanence and very slow relaxation evidenced on larger time-scales after $0.5 \cdot 10^4$ s demonstrate the reduced pathways for charge annihilation and characterizes again the purely interfacial bidimensional nature of the transport evidenced here.

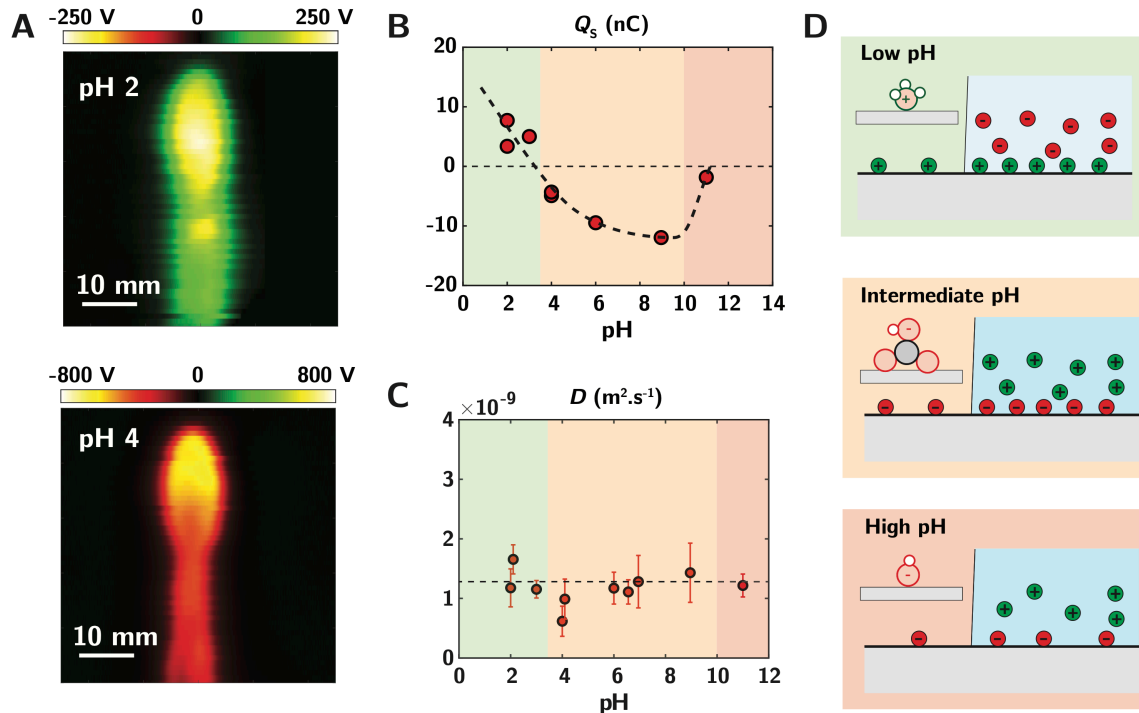


Figure 4. Physicochemical control of charge deposition and surface diffusion. (A) Surface potential maps obtained through successive droplet sliding at pH 2 and pH 4, showing reversal of the deposited charges. pH is adjusted in a solution with 10 mM KCl background salt (see SI.S1). (B) Evolution of the surface charge Q_s with droplet pH. The dashed line is a guide to the eyes. (C) Surface charge diffusion coefficient D as a function of pH. (D) Envisioned mechanism for surface charging, associated with the color-coded regime in (B) and (C), with the adsorption of H_3O^+ , HCO_3^- and OH^- at respectively low, intermediate and high pH values.

Liquid physicochemistry can tune surface charging

These peculiar observations raise the question of the physicochemical state of these surface deposited charges and their relation with ionic adsorption at the solid/liquid interface close to the dewetting contact line. To probe this question in more detail, we investigate the effect of liquid physicochemistry on charge deposition. We probed in particular the effect of pH, using solutions with a background level of 10 mM salt, in order to keep the Debye screening length constant of the entire range of studied pH. As evidenced in Fig. 4A, we observe a dramatic effect of pH on surface charging, with a switch in the sign of the deposited surface charge when decreasing the pH to acidic values. This trend is confirmed in Fig. 4B, where we report the evolution of the total surface charge Q_s [C] as a function of the droplet pH, showing a reversal from positive to negative charging around pH 3.5. Interestingly, the general observed trend is consistent with surface (or zeta) potential evolution typically evidenced in water on various hydrophobic surface [26]. Surprisingly, while this general trend for hydrophobic surface charging has been reported in a robust manner, the exact charging mechanisms of hydrophobic surfaces remain unclear [27]. Original interpretations pointed to the role of the specific interfacial adsorption of water self-ions H_3O^+ and OH^- on surface charging at respectively low and high pH values [28]–[30]. Concurrent explanation involves the specific adsorption of

hydrogenocarbonate ions, originating from CO_2 dissolution at neutral to basic pH [31], as well as surface-specific impurities [32], [33] or reorganization in the interfacial hydrogen-bonding network of water [34]–[36]. In our case, we observe a decrease of the deposited charge when reaching large pH (Fig. 4B and Fig. S7), coinciding with the pK_a of 10.3 for the equilibrium between HCO_3^- and CO_3^{2-} . This observation suggests that ions originating from dissolved gaseous CO_2 play a key role on surface charging process at intermediate pH. The situation envisioned can then be schematically represented with the three colored domains in Fig. 4B and 4D, with H_3O^+ , HCO_3^- and OH^- as the dominant surface-active species at respectively low (green), intermediate (orange) and high (red) pH.

We might expect the presence of these distinct species to affect interfacial mobility. In bulk water at 25°C , the mobilities of these various ions can indeed vary by a factor of 10 from $9.4 \cdot 10^{-9} \text{ m}^2 \cdot \text{s}^{-1}$ and $5.2 \cdot 10^{-9} \text{ m}^2 \cdot \text{s}^{-1}$ for H_3O^+ and OH^- [37] down to $1.2 \cdot 10^{-9} \text{ m}^2 \cdot \text{s}^{-1}$ for HCO_3^- [38]. These differences are attributable to the peculiar mode of diffusion for H_3O^+ and OH^- , which does not involve Fickian-like drag of the ionic center of mass, but rather involves Grotthus hopping and tunneling of the excess proton from water molecules to water molecules leading to ultrafast transport. Remarkably, such large modulation of the ionic mobility *at the interface* is not recovered in our experiments, with a constant diffusion coefficient across the various pH values (Fig. 4C). These two observations of (i) a diffusion process independent of the exact ionic nature and (ii) mobility values which can exceed standard bulk ionic diffusion coefficient for simple ions suggest the occurrence of a peculiar mode for 2D ionic transport at solid/gas interfaces, which we will address in the following discussion.

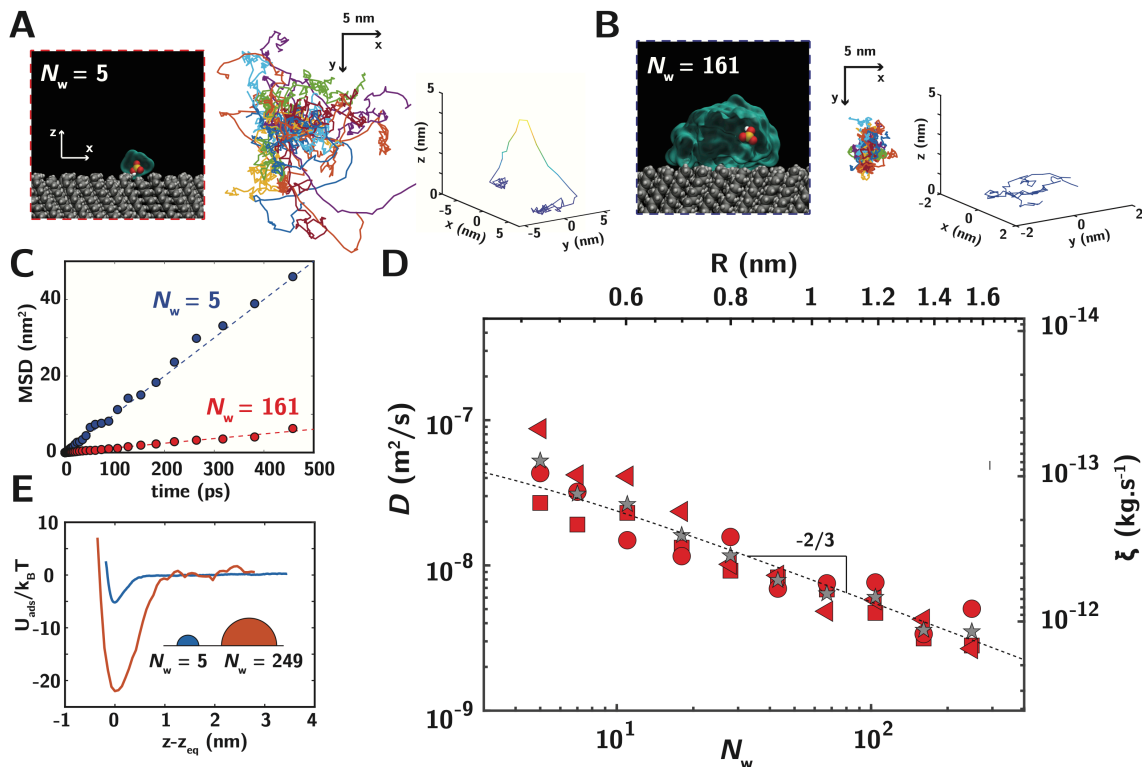


Figure 5. Molecular insight into interfacial ionic diffusion. (A-B) Snapshot of MD simulations for a surface adsorbed ion surrounded by hydration shell with $N_w = 5$ and 161 water molecules (left panel), along with typical 0.5 ns trajectories, projected on the (xy) plane (center panel) and examples of single trajectories in (xyz), with the vertical z position color-coded according to height from blue to yellow (right panel), showing the occurrence of transient detachment out of the surface for $N_w = 5$ in (A). (C) Effective Mean-Squared Displacement (MSD) as a function of time for the two equilibrium states depicted in (A) (averaged over 30 independent simulations). (D) Evolution of diffusion coefficient with the number of physisorbed water molecules. The dashed line represents a power-law scaling of $-2/3$, and the different symbols correspond respectively to OH^- (triangles), H_3O^+ (circles) and HCO_3^- (squares). Grey stars indicate the averaged diffusion coefficient for these three species. (E) Interfacial

physisorption energy $U_{\text{ads}}/k_{\text{B}}T$ for a bicarbonate ion surrounded by 5 and 249 water molecules. z_{eq} characterizes the equilibrium position at which U_{ads} is minimal.

Ionic transport is limited by interfacial hydrated friction

A question arises with respect to the physicochemical state of these surface adsorbed ions. Although trapped at the solid/gas interface, we might expect these ions to still be surrounded by a few water molecules, due to the high enthalpic cost of $50 k_{\text{B}}T$ needed to fully strip away their water hydration shell [4], [39]. With this picture in mind, we turn to molecular dynamics simulation in Fig. 5 to get more insights into the possible molecular transport mechanisms for these mobile surface adsorbed ions. As shown in Fig. 5A, we consider the dynamics of a single ion (here a bicarbonate HCO_3^- ion) adsorbed on a hydrophobic self-assembled monolayer surface. We consider these ions under distinct hydration levels, characterized by the number N_{w} of water molecules adsorbed around them, with here respectively $N_{\text{w}} = 5$ and 161 water molecules, a range justified by Grand Canonical simulations at various relative humidity (Fig. S8).

As shown in SI Movie S1-2, we let these hydrated ions evolve spontaneously at the interface, evidencing a random diffusive-like surface motion (see individual trajectories in Fig. 5A-B). At a qualitative level, we already evidence significant difference in charge mobility for distinct hydration level, with the largest nanodroplets displaying slower dynamics (comparing trajectories shown in the center plot in Figs. 5A and B). Interestingly, while the motion for the large ionic nanodroplet is purely confined in 2D at the interface (B, left panel), for the weakly hydrated ion, we evidenced the occurrence of transient detachments from the surface followed by flights in the vapor (A, left panel showing a 3D trajectory), an effect we return to later.

To characterize these differences of dynamics in more quantitative terms, we compute in Fig. 5C the temporal evolution of the Mean-Squared Displacement, from which the associated 2D diffusion coefficient D_{ion} [$\text{m}^2 \cdot \text{s}^{-1}$] is obtained as $\langle (\mathbf{x}(t) - \mathbf{x}_{t=0})^2 \rangle = 4D_{\text{ion}}t$, leading to diffusion coefficients spanning over one order of magnitude, from $D_{\text{ion}} \approx 2.5 \cdot 10^{-8} \text{ m}^2 \cdot \text{s}^{-1}$ to $D_{\text{ion}} \approx 3 \cdot 10^{-9} \text{ m}^2 \cdot \text{s}^{-1}$, when the number of water molecules increases from 5 to 250 (Fig. 5D). A first comment arises regarding the order of magnitude of these associated diffusion coefficients, which are found to be up to one order of magnitude larger than in bulk water, highlighting the very small friction experienced by these surface physisorbed hydrated ions.

To analyze these effects in more detail and evidence the limiting transport steps in relation to ionic hydration, we plot in Fig. 5D the evolution of the diffusion coefficient as a function of the number of water molecules N_{w} . Interestingly, the surface diffusion coefficient D_{ion} follows a clear power-law decrease with N_{w} , associated with the approximate scaling $D_{\text{ion}} \sim N_{\text{w}}^{-2/3}$, shown by the dotted line in Fig. 5D. The approximate surface and volume of the drop scales respectively as $N_{\text{w}}^{2/3}$ and N_{w} . Hence, the scaling $D_{\text{ion}} \sim N_{\text{w}}^{-2/3}$ suggests an interface limited transport process, reminiscent of previous experimental [40] and computational studies [41], [42].

Building upon this idea of interfacially-limited transport, we write the diffusion coefficient as $D_{\text{ion}} = kT/\xi_{\text{ion}}$ with ξ_{ion} [$\text{kg} \cdot \text{s}^{-1}$] the friction coefficient of the hydrated ion, evolving within the range 10^{-13} to $10^{-12} \text{ kg} \cdot \text{s}^{-1}$ (Fig. 5D, right y-axis). Following up on the observed scaling in Fig. 5D, we express the ionic friction coefficient as $\xi_{\text{ion}} = A \cdot \lambda$, the product of the nanodroplet surface area A [m^2] by an interfacial friction coefficient λ [$\text{kg} \cdot \text{s}^{-1} \cdot \text{m}^{-2}$]. This friction coefficient depends on the specific liquid/surface interactions, and is readily related to the more commonly used slip length b [m], with $\lambda = \eta/b$ and η the liquid viscosity. Comparing this simple scaling with our computational results, we extract an interfacial friction coefficient $\lambda \approx 1.8 \cdot 10^5 \text{ Pa} \cdot \text{s} \cdot \text{m}^{-1}$, associated with a slip length $b = 5.5 \text{ nm}$. This effective slip length characterizing interfacial friction is in fair agreement with the OTS/water slip length of 1.5 nm measured independently in our simulations (see SI.S5), validating our conceptual approach.

Note that this scaling is expected to break down in the limit of ultra-low slip length for which the droplets might adopt a rolling-like motion, opening additional volumic dissipation channels, related to bulk nanodroplet deformation [43].

Returning to the 3D trajectories shown in Figs. 5AB, our simulations evidence a second unexpected mode of transport at play for very small nanodroplets, whereby the solvated ion can detach from the surface and undergo 3D flights (right panel in Fig. 5B). This transport mode cannot be fully characterized in our simulation due to the finite size of the simulation box, however they indicate a peculiar hopping and flying transport mode, which could significantly enhance the effective ionic diffusion. To characterize the possibility for thermally activated surface desorption, we quantify in Fig. 5D the effective adsorption energy of the solvated ion on the solid surface for solvation shells consisting of 5 and 250 water molecules, evidencing a typical adsorption energy U_{ads} of 4 and 25 $k_B T$ respectively. Assuming a molecular attempt probability of 10^{12} s^{-1} , we find a typical desorption rate of 6 ns^{-1} for the smallest drop, in fair agreement with our computational observations (see Fig. S9). Such desorption-mediated hopping mode might thus be expected to speed up interfacial transport significantly, particularly in the limit of low hydration number.

Hence, we evidenced the occurrence of a peculiar transport mechanism for surface adsorbed ions, associated with an interfacially limited frictional transport process clearly different from that observed for ionic transport in bulk water. At a qualitative level, these conclusions are consistent with our two experimental observations of (i) a diffusion process independent of the exact ionic nature and (ii) mobility values which can exceed the standard bulk ionic diffusion coefficient for simple ions. The range of diffusion coefficients measured experimentally ($D \approx 1 - 7 \cdot 10^{-9} \text{ m}^2 \cdot \text{s}^{-1}$) falls within the lower range of our simulations, predicting $D \approx 3 \cdot 10^{-9} \text{ m}^2 \cdot \text{s}^{-1}$ for a nanodroplet of 1.6 nm radius (Fig. 5E, upper axis). A fully quantitative comparison with our experiments is however currently out of reach, as the effective surface transport should be set by a combination of both ionic solvation and water/substrate friction, two quantities whose exact values remain unknown in our experiments. Note also that we could have expected the level of water adsorption around surface adsorbed ions to be affected by changes in the relative humidity, with an effect on the screening of the effectively measured surface potential. However, we did not evidence any change in the charge relaxation kinetics nor of the steady-state charge density with humidity. Consistent with this observation, the surface diffusion coefficient remains also independent of the relative humidity (SI Fig. S6).

Conclusion

Harvesting an in-situ scanning based potential mapping approach, we revealed the spatiotemporal evolution of surface-trapped charges deposited in the wake of droplets sliding down inclined hydrophobic surfaces. We showed that the deposited charge can be reversibly tuned by the bulk droplet pH, pointing to the role of water self-ion and dissolved CO_2 in the surface charging mechanism. Remarkably, the charges initially deposited along the wake of the droplet tend to spread apart on the solid surface over time, consistent with a bidimensional diffusion process associated with ultra-high 2D gliding mobility exceeding that of standard salt in bulk water. MD simulations rationalize our observations by revealing a peculiar mechanism for the transport of hydrated ions adsorbed on solid surfaces, uncorrelated to bulk transport properties and set by purely interfacial frictional interactions between the water molecules solvating these ionic charges and the solid surface.

Our observations and findings open up several exciting avenues and perspectives. In the context of solid electrification, the role of water adsorbates and mobile surface-adsorbed ions have been put forward to rationalize the charging of dielectric materials involving non-ionizable and ionizable polymer and hydrophobic materials [44]–[48], echoing the molecular picture presented here. Our measurements further stress that spatially and temporally resolved mapping

are necessary to properly assess charge relaxation processes in liquid triboelectrification [18]. The dynamics of this new state of interfacial ionic matter further raises fundamental questions in the context of iontronics and nanofluidics. We can mention among others the role played by solvation on interfacial ionic friction [49], the possibility for electrostatic stabilization of molecular water layers at hydrophobic interface [50], the role of electronic interactions during droplet friction on conductive surfaces [6], [51], [52], up to the possibility for peculiar physical processes such as ionic pairing at these low-permittivity air interfaces [53]. The *ionic puddles* evidenced here have accordingly thus just started to reveal their secrets.

Acknowledgement

Z.B. and J.C. thank ESPCI PSL for funding the position of Z.B as a Teaching and Research Fellow. J.C. acknowledge funding from the ANR (grant 'GUACAmole' ANR-22-CE06-0003-01). This project has also received financial support from the CNRS through the MITI interdisciplinary programs and from the Carnot Institute 'IPGG Microfluidique'. S.G. acknowledges access to the HPC resources of IDRIS under the allocation 2023-AD012A14560 made by GENCI.

Data availability

The data that support the findings of this study are available from the corresponding author, upon reasonable request. Simulation input files are available on GitHub, under the <https://github.com/simongravelle/publication-data> repository [Gravelle, S. simongravelle/publication-data: 3Mar2025. 2025; <https://doi.org/10.5281/zenodo.13341067>]

Supplementary Materials

Movie S1. A droplet consisting of a single bicarbonate ion (red, yellow, and white beads) and 5 water molecules (transparent field) on a layer of C₁₈ molecules (dark and light beads). The movie represents a duration of 200 ps, with a time interval of 0.2 ps between consecutive frames.

Movie S2. A droplet consisting of a single bicarbonate ion (red, yellow, and white beads) and 161 water molecules (transparent field) on a layer of C₁₈ molecules (dark and light beads). The movie represents a duration of 200 ps, with a time interval of 0.2 ps between consecutive frames.

Bibliography

- [1] D. J. Lacks and T. Shinbrot, "Long-standing and unresolved issues in triboelectric charging," *Nat. Rev. Chem.*, 2019.
- [2] M. W. Williams, "What creates static electricity?," *Am. Sci.*, vol. 100, no. 4, pp. 316–323, 2012.
- [3] T. Steinpilz *et al.*, "Electrical charging overcomes the bouncing barrier in planet formation," *Nat. Phys.*, vol. 16, no. 2, pp. 225–229, 2020.
- [4] A. Z. Stetten, D. S. Golovko, S. A. L. Weber, and H. J. Butt, "Slide electrification: Charging of surfaces by moving water drops," *Soft Matter*, vol. 15, no. 43, pp. 8667–8679, 2019.
- [5] M. D. Sosa *et al.*, "Liquid-polymer triboelectricity: Chemical mechanisms in the contact electrification process," *Soft Matter*, vol. 16, no. 30, pp. 7040–7051, 2020.
- [6] X. Li *et al.*, "Spontaneous charging affects the motion of sliding drops," *Nat. Phys.*, vol. 18, no. 6, pp. 713–719, 2022.
- [7] A. D. Ratschow, L. S. Bauer, P. Bista, S. A. L. Weber, H. J. Butt, and S. Hardt, "How Charges Separate when Surfaces Are Dewetted," *Phys. Rev. Lett.*, vol. 132, no. 22, p.

- 224002, 2024.
- [8] X. Li, A. D. Ratschow, S. Hardt, and H. J. Butt, "Surface Charge Deposition by Moving Drops Reduces Contact Angles," *Phys. Rev. Lett.*, vol. 131, no. 22, p. 228201, 2023.
 - [9] A. D. Ratschow, H.-J. Butt, S. Hardt, and S. A. L. Weber, "Liquid slide electrification : advances and open questions," *Soft Matter*, 2025.
 - [10] S. Lin, X. Chen, and Z. L. Wang, "Contact Electrification at the Liquid-Solid Interface," *Chem. Rev.*, vol. 122, no. 5, pp. 5209–5232, 2022.
 - [11] J. Nauruzbayeva, Z. Sun, A. Gallo, M. Ibrahim, J. C. Santamarina, and H. Mishra, "Electrification at water–hydrophobe interfaces," *Nat. Commun.*, vol. 11, no. 1, pp. 1–10, 2020.
 - [12] D. Choi *et al.*, "Spontaneous electrical charging of droplets by conventional pipetting," *Sci. Rep.*, vol. 3, pp. 1–7, 2013.
 - [13] S. Kooij, C. van Rijn, N. Ribe, and D. Bonn, "Self-charging of sprays," *Sci. Rep.*, vol. 12, no. 1, pp. 1–11, 2022.
 - [14] N. Miljkovic, D. J. Preston, R. Enright, and E. N. Wang, "Electrostatic charging of jumping droplets," *Nat. Commun.*, vol. 4, pp. 1–9, 2013.
 - [15] Q. Sun *et al.*, "Surface charge printing for programmed droplet transport," *Nat. Mater.*, vol. 18, no. 9, pp. 936–941, 2019.
 - [16] W. Xu *et al.*, "A droplet-based electricity generator with high instantaneous power density," *Nature*, vol. 578, no. 7795, pp. 392–396, 2020.
 - [17] Z. Zhang *et al.*, "Emerging hydrovoltaic technology," *Nat. Nanotechnol.*, vol. 13, no. 12, pp. 1109–1119, 2018.
 - [18] S. Lin, L. Xu, A. Chi Wang, and Z. L. Wang, "Quantifying electron-transfer in liquid-solid contact electrification and the formation of electric double-layer," *Nat. Commun.*, vol. 11, no. 1, pp. 1–8, 2020.
 - [19] Y. Jin *et al.*, "How liquids charge the superhydrophobic surfaces," *Nat. Commun.*, vol. 15, no. 1, pp. 1–8, 2024.
 - [20] J. Nie *et al.*, "Probing Contact-Electrification-Induced Electron and Ion Transfers at a Liquid–Solid Interface," *Adv. Mater.*, vol. 32, no. 2, 2020.
 - [21] K. Yatsuzuka, Y. Mizuno, and K. Asano, "Electrification phenomena of pure water droplets dripping and sliding on a polymer surface," *J. Electrostat.*, vol. 32, no. 2, pp. 157–171, 1994.
 - [22] J. V. Ross, "Stochastic models for mainland-island metapopulations in static and dynamic landscapes," *Bull. Math. Biol.*, vol. 68, no. 2, pp. 417–449, Feb. 2006.
 - [23] L. Bocquet and E. Charlaix, "Nanofluidics, from bulk to interfaces," *Chem. Soc. Rev.*, vol. 39, no. 3, pp. 1073–1095, 2010.
 - [24] M. C. Audry, A. Piednoir, P. Joseph, and E. Charlaix, "Amplification of electro-osmotic flows by wall slippage: Direct measurements on OTS-surfaces," *Faraday Discuss.*, vol. 146, pp. 113–124, 2010.
 - [25] V. Vitagliano and P. A. Lyons, "Diffusion Coefficients for Aqueous Solutions of Sodium Chloride and Barium Chloride," *J. Am. Chem. Soc.*, vol. 78, no. 8, pp. 1549–1552, 1956.
 - [26] R. Zimmermann, U. Freudenberg, R. Schweiß, D. Küttner, and C. Werner, "Hydroxide and hydronium ion adsorption - A survey," *Curr. Opin. Colloid Interface Sci.*, vol. 15, no. 3, pp. 196–202, 2010.
 - [27] Y. Uematsu, "Electrification of water interface," *J. Phys. Condens. Matter*, vol. 33, no. 42, pp. 1–23, 2021.
 - [28] R. Zimmermann, S. Dukhin, and C. Werner, "Electrokinetic Measurements Reveal Interfacial Charge at Polymer Films Caused by Simple Electrolyte Ions," *J. Phys. Chem. B*, vol. 105, no. 36, pp. 8544–8549, 2001.
 - [29] K. N. Kudin and R. Car, "Why are water-hydrophobic interfaces charged?," *J. Am.*

- Chem. Soc.*, vol. 130, no. 12, pp. 3915–3919, 2008.
- [30] C. S. Tian and Y. R. Shen, “Structure and charging of hydrophobic material/water interfaces studied by phase-sensitive sum-frequency vibrational spectroscopy,” *Proc. Natl. Acad. Sci. U. S. A.*, vol. 106, no. 36, pp. 15148–15153, 2009.
- [31] X. Yan *et al.*, “Central Role of Bicarbonate Anions in Charging Water/Hydrophobic Interfaces,” *J. Phys. Chem. Lett.*, vol. 9, no. 1, pp. 96–103, 2018.
- [32] Y. Uematsu, D. J. Bonthuis, and R. R. Netz, “Nanomolar Surface-Active Charged Impurities Account for the Zeta Potential of Hydrophobic Surfaces,” *Langmuir*, vol. 36, no. 13, pp. 3645–3658, 2020.
- [33] Y. Uematsu, D. J. Bonthuis, and R. R. Netz, “Impurity effects at hydrophobic surfaces,” *Curr. Opin. Electrochem.*, vol. 13, pp. 166–173, 2019.
- [34] S. Pullanchery, S. Kulik, B. Rehl, A. Hassanali, and S. Roke, “Charge transfer across C–H···O hydrogen bonds stabilizes oil droplets in water,” *Science (80-.)*, vol. 374, no. 6573, pp. 1366–1370, 2021.
- [35] R. Vácha, O. Marsalek, A. P. Willard, D. J. Bonthuis, R. R. Netz, and P. Jungwirth, “Charge transfer between water molecules as the possible origin of the observed charging at the surface of pure water,” *J. Phys. Chem. Lett.*, vol. 3, no. 1, pp. 107–111, 2012.
- [36] E. Poli, K. H. Jong, and A. Hassanali, “Charge transfer as a ubiquitous mechanism in determining the negative charge at hydrophobic interfaces,” *Nat. Commun.*, vol. 11, no. 1, pp. 1–13, 2020.
- [37] M. Chen *et al.*, “Hydroxide diffuses slower than hydronium in water because its solvated structure inhibits correlated proton transfer,” *Nat. Chem.*, vol. 10, no. 4, pp. 413–419, 2018.
- [38] R. E. Zeebe, “On the molecular diffusion coefficients of dissolved CO₂, HCO₃⁻, and CO₃²⁻ and their dependence on isotopic mass,” *Geochim. Cosmochim. Acta*, vol. 75, no. 9, pp. 2483–2498, 2011.
- [39] P. Loche, D. J. Bonthuis, and R. R. Netz, “Molecular dynamics simulations of the evaporation of hydrated ions from aqueous solution,” *Commun. Chem.*, vol. 5, no. 1, pp. 1–8, 2022.
- [40] C. Ritter, M. Heyde, B. Stegemann, K. Rademann, and U. D. Schwarz, “Contact-area dependence of frictional forces: Moving adsorbed antimony nanoparticles,” *Phys. Rev. B - Condens. Matter Mater. Phys.*, vol. 71, no. 8, pp. 1–7, 2005.
- [41] M. Ma, G. Tocci, A. Michaelides, and G. Aeppli, “Fast diffusion of water nanodroplets on graphene,” *Nat. Mater.*, vol. 15, no. 1, pp. 66–71, 2016.
- [42] L. J. Lewis, P. Jensen, N. Combe, and J. L. Barrat, “Diffusion of gold nanoclusters on graphite,” *Phys. Rev. B - Condens. Matter Mater. Phys.*, vol. 61, no. 23, pp. 16084–16090, 2000.
- [43] J. Servantie and M. Müller, “Statics and dynamics of a cylindrical droplet under an external body force,” *J. Chem. Phys.*, vol. 128, no. 1, pp. 1–11, 2008.
- [44] V. Lee, N. M. James, S. R. Waitukaitis, and H. M. Jaeger, “Collisional charging of individual submillimeter particles: Using ultrasonic levitation to initiate and track charge transfer,” *Phys. Rev. Mater.*, vol. 2, no. 3, p. 035602, 2018.
- [45] L. S. McCarty and G. M. Whitesides, “Electrostatic charging due to separation of ions at interfaces: Contact electrification of ionic electrets,” *Angew. Chemie - Int. Ed.*, vol. 47, no. 12, pp. 2188–2207, 2008.
- [46] S. Pence, V. J. Novotny, and A. F. Diaz, “Effect of Surface Moisture on Contact Charge of Polymers Containing Ions,” *Langmuir*, vol. 10, no. 2, pp. 592–596, 1994.
- [47] J. A. Wiles, M. Fialkowski, M. R. Radowski, G. M. Whitesides, and B. A. Grzybowski, “Effects of surface modification and moisture on the rates of charge transfer between

- metals and organic materials,” *J. Phys. Chem. B*, vol. 108, no. 52, pp. 20296–20302, 2004.
- [48] L. S. McCarty, A. Winkleman, and G. M. Whitesides, “Ionic electrets: Electrostatic charging of surfaces by transferring mobile ions upon contact,” *J. Am. Chem. Soc.*, vol. 129, no. 13, pp. 4075–4088, 2007.
- [49] S. Goutham *et al.*, “Beyond steric selectivity of ions using ångström-scale capillaries,” *Nat. Nanotechnol.*, vol. 18, no. 6, pp. 596–601, 2023.
- [50] A. Allemand *et al.*, “Anomalous ionic transport in tunable angstrom-size water films on silica,” *Proc. Natl. Acad. Sci. U. S. A.*, vol. 120, no. 25, 2023.
- [51] M. Lizée *et al.*, “Strong Electronic Winds Blowing under Liquid Flows on Carbon Surfaces,” *Phys. Rev. X*, vol. 13, no. 1, pp. 1–12, 2023.
- [52] J. Yin, X. Li, J. Yu, Z. Zhang, J. Zhou, and W. Guo, “Generating electricity by moving a droplet of ionic liquid along graphene,” *Nat. Nanotechnol.*, vol. 9, no. 5, pp. 378–383, 2014.
- [53] D. Toquer, L. Bocquet, and P. Robin, “Ionic association and Wien effect in 2D confined electrolytes,” *J. Chem. Phys.*, vol. 162, no. 6, 2025.